Science of the Total Environment 1009 (2025) 181063

Contents lists available at ScienceDirect

Science of the Total Environment

journal homepage: www.elsevier.com/locate/scitotenv

Enhancement of coastal flood mitigation by implementing hybrid flood defences integrating hard engineering and nature-based solutions

Constantinos Matsoukis [a,*], Marta Payo Payo [a], Jennifer Brown [b], Laurent Amoudry [a]

[a] National Oceanography Centre, Joseph Proudman Building, 6 Brownlow Street, Liverpool, L3 5DA, UK
[b] National Oceanography Centre, European Way, Southampton, SO14 3ZH, UK

HIGHLIGHTS

- Our case study indicates that hybrid defences could be effective against storm tides.
- Loss of agricultural land can be limited when implementing hybrid solutions.
- Vegetation reduces flooding when interfering with the prevalent flow circulation.

GRAPHICAL ABSTRACT

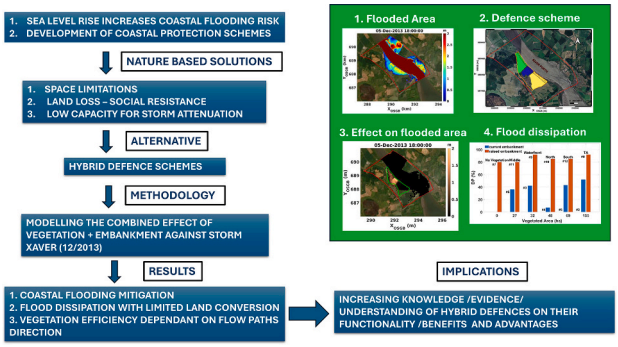

ARTICLE INFO

Keywords:
Coastal flooding
Nature-based solutions
Hybrid defences
Vegetation
Storm attenuation

ABSTRACT

Due to the energy dissipation induced by vegetation, restoration of natural ecosystems such as salt marshes is often considered an attractive nature-based solution against coastal flooding as an alternative to hard engineered defences. Even though this vegetation's capacity to dissipate energy has been well affirmed in the literature for short waves, it is still disputed for long waves (i.e., storm surges and tides) resulting in significant uncertainty on the potential effectiveness of mitigating the impact of storm surges. Furthermore, restoration or creation of coastal habitats often face challenges due to space limitations and social resistance linked to loss of valuable land. Hybrid schemes, integrating existing hard defences and natural solutions (e.g., vegetation zones), could be a good alternative to overcome such problems. However, evidence to support their implementation and design is lacking.

In this study, a modelling chain in Delft3D-FM has been implemented to test the efficiency of a hybrid solution consisting of an embankment and vegetation zones in a case study in the inner Forth estuary (Scotland, UK). The flood protection effectiveness of the proposed solution is assessed for the storm Xaver (December 2013) that greatly affected the area. The model results indicate that the proposed hybrid scheme could considerably reduce the land loss for coastal protection and that the effect of vegetation depends on design criteria such as position and orientation relative to the prevalent current flow. These results provide valuable insight towards applicability, design and implementation of hybrid schemes.

* Corresponding author.
E-mail address: conmat@noc.ac.uk (C. Matsoukis).

https://doi.org/10.1016/j.scitotenv.2025.181063
Received 14 July 2025; Received in revised form 21 November 2025; Accepted 23 November 2025
Available online 28 November 2025
0048-9697/© 2025 The Authors. Published by Elsevier B.V. This is an open access article under the CC BY license (http://creativecommons.org/licenses/by/4.0/).

1. Introduction

Coastal flooding is a threat to the almost 1 billion people estimated globally to live within 10 km of the coast (Reimann et al., 2023). Sea level rise (SLR) increases the risk of flooding as higher coastal water depths mean that even moderate surges may overtop the current coastal defences (Chen et al., 2024; De Dominicis et al., 2020; Haigh et al., 2017). Storm events such as hurricanes Katrina (2004) and Sandy (2012) in the United States (Yin et al., 2016), storms Xynthia (2010) and Xaver (2013) in Europe (Haigh et al., 2017), Jebi and Trami in Japan (Yamanaka et al., 2019) or Yagi in South East Asia (He et al., 2025) resulted in human casualties and caused heavy financial losses. Hence, the development of coastal protection schemes to protect the most vulnerable areas from similar or even more extreme events has become imperative.

In recent years, coastal practitioners globally are shifting from traditional hard coastal defences (e.g., breakwaters, seawalls, revetments, groynes etc.) in favour of 'greener' nature-based solutions (Sutton-Grier et al., 2015) that involve management, restoration or creation of natural ecosystems along coastlines to protect against flooding and erosion (Schoutens et al., 2020). The restored habitats (e.g., salt marshes) can then act as buffers and mitigate storm impact because of the vegetation's capacity to dissipate wave energy (Temmerman et al., 2023).

As storms propagate landward, vegetation exerts friction that decreases flow velocity and turbulence causing wave damping and lower peak water levels (Temmerman et al., 2023). Coastal elevation can also increase because of the vegetation's ability to trap sediments (Baaij et al., 2021). The effectiveness of vegetation to attenuate storm energy may depend on bathymetry and large-scale landscape (e.g., the presence of channels, barrier islands, dikes or levees etc.), wetland structure (i.e., thickness, density and height) and storm characteristics (i.e., intensity, duration and speed) (Chen et al., 2021; Sheng et al., 2021). The ability of vegetation to attenuate short waves (i.e., wind waves, swells) has been demonstrated in several studies (Möller et al., 2014; Schoutens et al., 2019; Yin et al., 2021; Maza et al., 2021). Conversely, long waves (i.e., storm surges and tides) might be less affected by the presence of vegetation (Schuerch et al., 2022). Temmerman et al. (2023) state that the storm surge attenuation rate is about two orders of magnitude smaller than that of surface wave attenuation rates: ~1 % per 100 m instead of 1 % per 1 m respectively. A decrease of attenuation rate with increasing wave period is further supported by meta-analyses (Gedan et al., 2011), numerical modelling (e.g., Zhao and Chen, 2016) and flume experiments (e.g., Rupprecht et al., 2017).

Usually, tens of kilometres of continuous marshes are needed for sufficient storm surge reduction (Leonardi et al., 2018). However, the substantial space requirement for ecosystems restoration or protection is not always possible causing serious limitation for natural approaches (Sutton-Grier et al., 2015). Lathrop et al. (2019) argued that the protection of communities from larger storms should explore the employment of a hybrid approach complementing existing natural habitats with additional engineering structures. There is increasing evidence of the flood protection benefits of hybrid approaches (e.g., Taylor-Burns et al., 2025; Du et al., 2020; Van Coppenolle et al., 2018).

Hybrid defences can take advantage of both 'grey' and 'green' solutions benefits while minimizing their drawbacks (Morris et al., 2018; Chen et al., 2024; Justine and Seenath, 2025a, 2025b) and are a good option in medium and high wave energy environments where it is expected that natural habitats would be less successful as coastal defences (Saleh and Weinstein, 2016). While fully natural solutions often face criticism and social resistance from communities at risk of flooding (Areia et al., 2023; Apine and Stojanovic, 2024; Seenath et al., 2025), hybrid solutions with even moderate engineering structures could provide a perception of safety (Sutton-Grier et al.,2015) making the implementation of flood management plans more acceptable to communities.

Despite growing interest in hybrid coastal defences, there is limited expertise and knowledge on their application (Sutton-Grier et al., 2015). Sparse evidence is available to support their effectiveness on storm mitigation and more research is needed to identify how, when and where to design such schemes (Sutton-Grier et al., 2015; Chen et al., 2024; Justine and Seenath, 2025a, 2025b). Previous studies (e.g., Chen et al., 2024) investigated the level of wave attenuation provided by a hybrid scheme but did not quantify its potential to decrease flood depths, extents and volumes.

Here, the response of a coastal system to a real storm event (Xaver, 2013), is modelled both with and without the presence of a hybrid coastal defence consisting of an embankment and vegetation zones. The case study focuses on the village of Airth, located in the inner Forth Estuary (Scotland, UK) which has a well-documented history of frequent flooding (see Section 2).

Airth's vulnerability and exposure to flooding have forced the local authorities to pursue effective flood management strategies. Several solutions have been considered. For instance, Austin et al. (2022) identified Airth as a potential location for Managed Realignment (MR) due to its potential for carbon sequestration. MR would involve breaching and landward relocation of an existing coastal embankment. However, the site presents several common blockers to MR making a hybrid defence an attractive alternative. The distance between the village and the river Forth (less than 1 km) is much less than required for effective storm attenuation. As is common in similar cases, MR faces strong social resistance from residents, farmers and landowners. The land between Airth and the estuary front is used for agriculture and local stakeholders are unwilling to give it up. In these aspects, the case study considered here typifies issues observed in many coastal settings and communities both within and beyond the UK.

This paper is organized as follows. Section 2 provides information on the case study and storm conditions under investigation. Section 3 includes the methodology (model setup, calibration and validation). The model results are presented in Section 4 and discussed in Section 5, followed by conclusions in the last section.

2. Case study

Airth is a village situated on the south bank of the inner Forth Estuary (Fig. 1) with a population of 1500 approximately covering an area of 22.4 km^2. It lies within a geomorphologically complex, macrotidal estuary characterised by vast intertidal areas and salt marshes (Table 1). It is a residential area that covers 5500 ha of agricultural land with most of it being in arable use. Beyond the farmland, salt marshes cover the foreshore over a width of 50 m to the river Forth. Surveys commissioned by the Scottish Natural Heritage (now Nature Scot) reveal that the salt marshes in the Forth estuary consist of three plants: *Puccinellia Maritima, Festuca Rubra* and *Jungus Gerurdii*.

Airth lies within one of the 30 potentially vulnerable areas to coastal flooding identified by the Scottish Environment Protection Agency (SEPA) in the Forth Estuary. The risk of coastal flooding in Airth is mainly associated with high sea levels due to stormy weather. Wind waves effects are minimal in this case because of wave transformation after the narrowing of the Forth Estuary (Fig. 2A and B). It is considered that about 290 people and 150 properties may be at risk of flooding by 2080s (SEPA, 2021). An area of 2.7 km^2 of agricultural land is also under threat of flooding together with critical infrastructure such as a local wastewater treatment works.

In the past, coastal flooding occurred several times along the Forth Estuary (e.g., 2002, 2010, 2012, 2013, 2014 and 2020) when high tides were combined with high storm surges (SEPA, 2021). Airth has been highly impacted by these events with storm Xaver being the most disastrous for the local community (see Section 2.1). Currently, the only protection from flooding is an earth embankment of approximately 2.5 km length along the estuary. However, the level of protection depends on the embankment's condition as it has often been damaged during

past flood events and needs frequent repairs.

2.1. Storm conditions

Storm Xaver (5–6 of December 2013) was the worst flooding event in the UK for more than half a century, only comparable to the storm surge of 1953 that devastated the coastal regions of Northwest Europe (Haigh et al., 2017). Enhanced by a low-pressure system over the Norwegian Sea, storm Xaver developed off the coast of Greenland on 3rd December 2013 and moved eastward towards the UK. It passed over Scotland on the 5th of December causing a cold air outbreak that led to gusty winds across the North Sea (Kettle, 2020). A minimum low pressure of ~1000 mbar was recorded along the east coast of the UK (Christakos et al., 2016; Wadey et al., 2015). Scotland was severely impacted by winds that gusted at 60–70 knots and affected railway services (Wadey et al., 2015) while intense wind-induced waves and extreme sea levels resulted to coastal flooding (Haigh et al., 2017).

In Airth, the combination of high tide and storm surge caused a breach of the existing flood defences allowing seawater to flood agricultural land and damage the local Wastewater Treatment Works (SEPA, 2021). During the event, the tide gauge at Leith (the closest to Airth, Fig. 2A), recorded a maximum water level of 3.42 m above Ordnance Datum on the 5th of December at 15:15 with a skew surge of 0.7 m (Kettle, 2020). At the mouth of the Forth estuary, the maximum significant wave height was approximately 2 m (Kettle, 2020). According to extreme sea level estimates by the Environment Agency (2018) and SEPA's flood risk maps, (https://map.sepa.org.uk/floodmap/map.htm), these conditions correspond to an event with a 5 % annual exceedance probability (a 1 in 20 year event, Wadey et al., 2015).

Table 1
Typical estuary geomorphological and hydrodynamic categories and habitats. Categories and habitats corresponding to the Forth Estuary and Airth are indicated by italics.

Geomorphology	Hydrodynamic	Habitats
Linear shore	River dominated	Mudflats/Sandflats
Coastal plain	Wave dominated	*Salt marshes*
Complex	Microtidal	Rock cliffs
Bar built	Mesotidal	Mangroves
Ria	*Macrotidal*	Seagrass
Deltaic		Tidal creeks
Embayment		*Arable land*

3. Methods

3.1. Numerical model

A 2D numerical model is built in Delft3D-Flow Flexible Mesh (D-FLOW FM) to determine the hydrodynamic setup in the Forth Estuary. D-FLOW FM comprises a fully integrated modelling suite capable of 1D, 2D and 3D simulations for hydrodynamics, waves, water flow and quality in coastal, estuarine and river areas. It solves the unsteady shallow water equations for an incompressible fluid under the Boussinesq assumption on an unstructured finite volume grid (Deltares, 2021). D-FLOW FM has been previously implemented successfully in studies for coastal and compound flooding (Nederhoff et al., 2021; Muñoz et al., 2022; Tang and Gallien, 2023; Lee et al., 2024).

3.1.1. Grid

A hybrid unstructured grid is constructed consisting of 33,960 elements with curvilinear cells in the river channel and estuary and

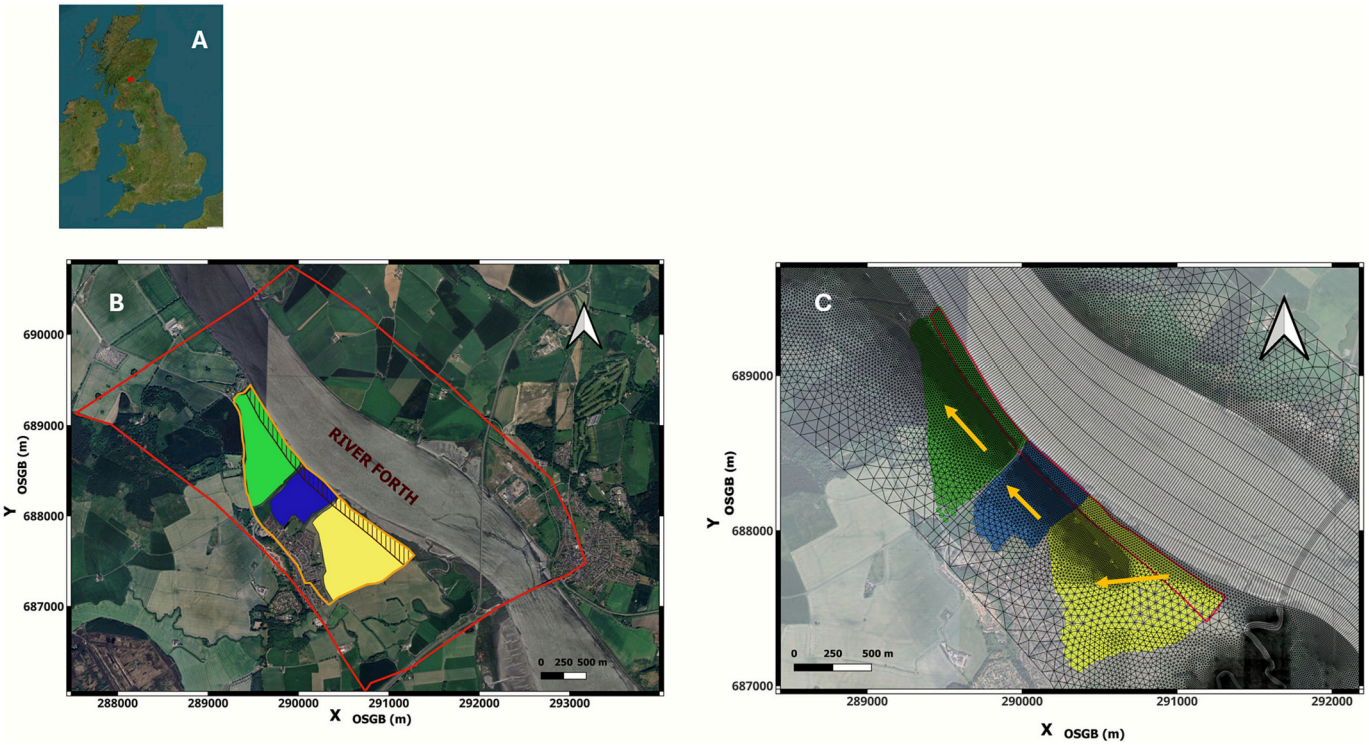

Fig. 1. A) UK's map where the red dot indicates the Airth's location. B) Aerial view of the Airth in the inner Forth estuary (basemap: Google Earth). The red and orange lines delineate the extents of the fine resolution model and of the area targeted (TA) by SEPA where measures need to be taken for coastal protection. The green, blue and yellow polygons depict the vegetation zones at the north, middle and south sections respectively. A water course and a narrow road separate these three sections. The hash polygon represents the vegetation zone in the Waterfront scenario. C) Zoom in the fine model grid. The coloured dots indicate the grid cells where a new roughness coefficient is measured based on Baptist (2005) equation, for the North (green), Middle (blue) and South (yellow) vegetation zones. The red line polygon encloses the grid cells with vegetation in the Waterfront scenario. All the coloured grid cells are considered in the target area scenario. The orange arrows indicate the dominant flow path in the reference scenario (Scenario 1).

triangular ones in the floodplains. This approach is in accordance with suggestions from the literature stating that this secures the optimum computational efficiency and level of output accuracy (Bomers et al., 2019; Muñoz et al., 2022). The model spans a longitudinal distance of 50 km approximately with the grid cells size increasing gradually from 30 m to 200 m between the outlet of the Forth catchment and the end of the inner Forth estuary (Fig. 2A). The model's lateral extents are determined so that they include inland areas with a 10 % chance of flooding based on flood maps provided by SEPA. These can be found at https://map.sepa.org.uk/floodmap/map.htm.

3.1.2. Bathymetry

The water depths in the Forth estuary are determined based on a digital marine elevation model (DMEM) provided by UK's Hydrographic Office (UK HO). The water depths are given relative to Chart Datum (CD) and are converted to Newlyn's Ordnance Datum (ODN) based on data from UK HO Vertical Offshore Reference Frame (VORF). Water depths along the river Forth are obtained by digitizing Scotland – East Coast - River Forth- Rosyth Marine Chart GB_GB50484C (available at https://www.gpsnauticalcharts.com/main/uk/folio7-north-sea-forth-thames-entrance-nautical-charts-folio.html). The river Forth's water depths are also converted to ODN. The marine chart provides depths in the river as far as Stirling (Fig. 2A).

3.1.3. Land elevation

Lidar data are used to determine the topography of inland areas based on a Digital Terrain Model (DTM) produced after a campaign that the Scottish government commissioned (available at https://remotesensingdata.gov.scot/). These data come with a resolution of 5 cm and cover coastal areas along the Forth Estuary. Online versions of UK's Ordnance Survey maps (https://digimap.edina.ac.uk/) are used to extract land elevation for inland areas along the river Forth.

3.1.4. Boundary conditions

The model is forced by time series of river discharges at the upstream boundary and water levels at the downstream boundary. River discharges are taken from a station deployed by SEPA at Craigforth (Fig. 3A). Water levels are taken from a tidal gauge at Leith (Fig. 3B) with data available from the British Oceanographic Data Centre (BODC). The locations of the stations can be seen in Fig. 2A. In both cases, river discharge and water levels are updated every 15 min. For simplicity, the water level is taken uniform along the downstream boundary. Freshwater input is added at four stations along the river Forth where river flow records are available from existing SEPA's stations (Fig. 2A).

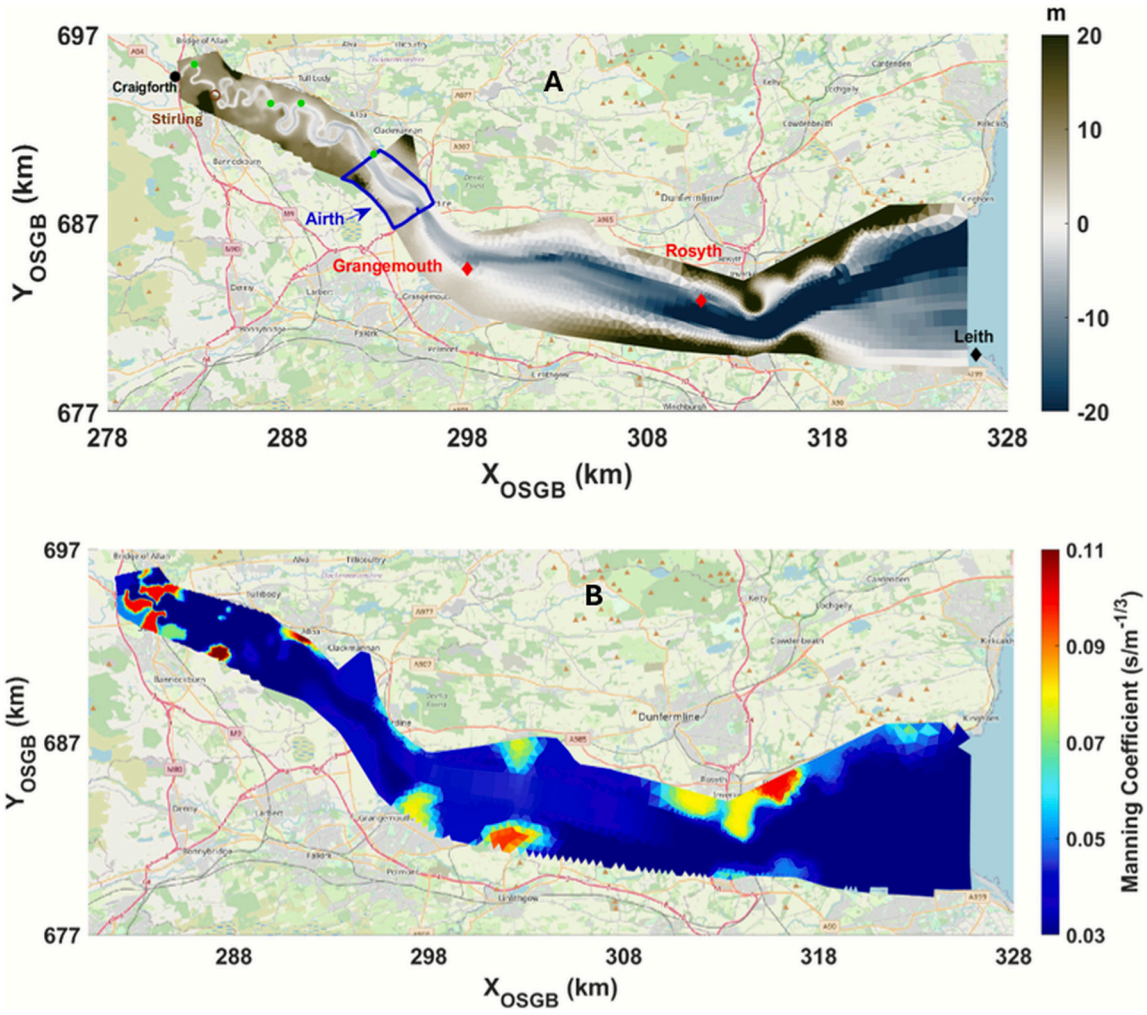

Fig. 2. A) Topo-bathymetry of the coarse model. Water depths and land elevation are given with respect to the Newlyn's Ordnance Datum (ODN). Circles indicate river discharge and diamonds water level stations. Black colour represents stations used to implement boundary conditions. The calibration stations are given with red colour, and green bullets display the locations with freshwater input along the river Forth. The blue line delineates the borders of the fine resolution model around the study area. The blue arrow points out where the Airth village lies. The brown unfilled circle is the point (at Stirling) up to where the mean sea level has been implemented as an initial condition. B) The spatially varying roughness field (Manning coefficients).

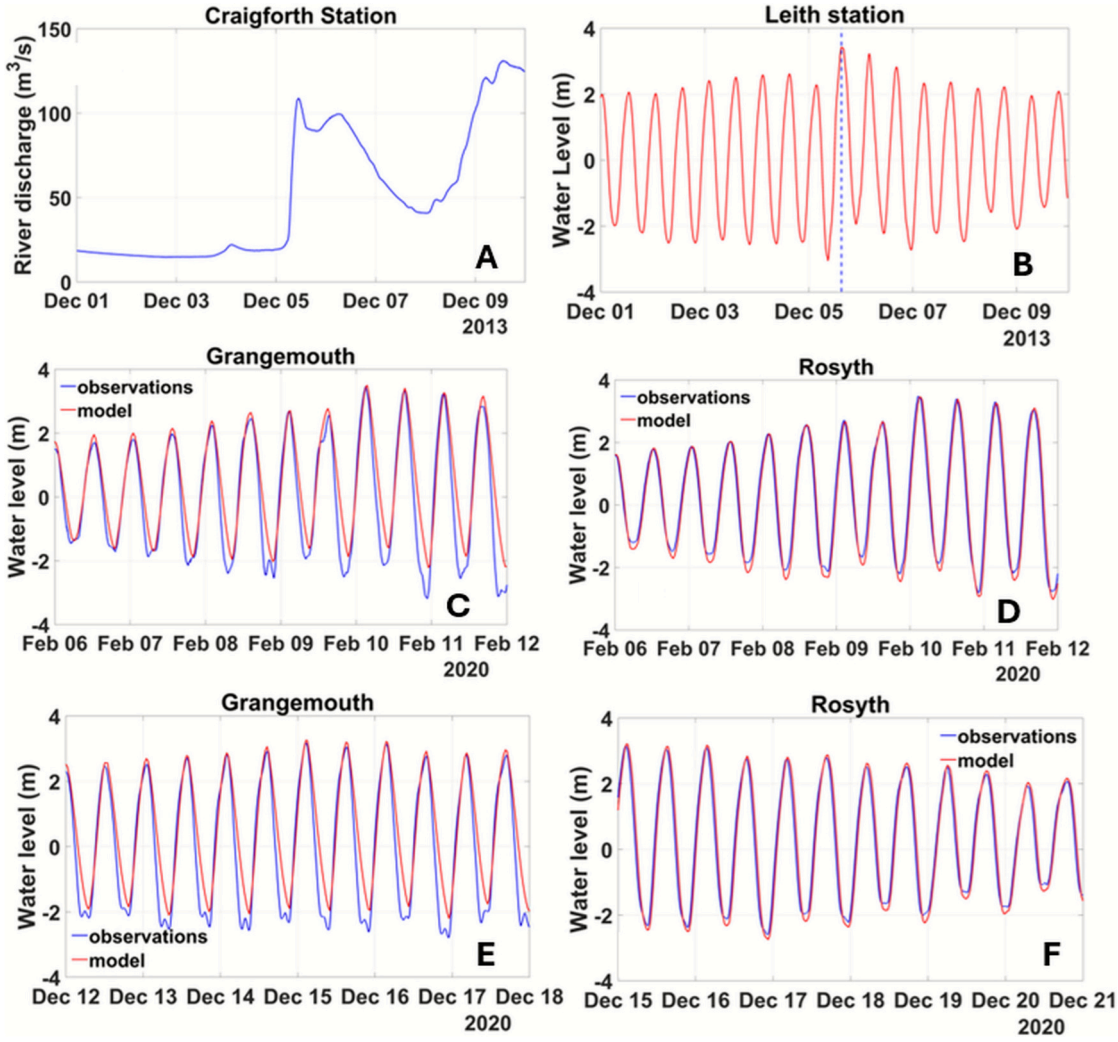

Fig. 3. Time series of A) river discharge and B) water level implemented at the upstream (Craigforth) and downstream (Leith) boundaries. The blue dashed vertical line indicates the time of the maximum water level implemented at the boundary. Water levels comparison for calibration (C, D) and validation (E, F) for the Grangemouth (left) and Rosyth (right) stations.

3.2. Initial conditions and model settings

The initial water level in the model simulations is taken equal to ODN between the downstream boundary (at Leith) and up to Stirling (Fig. 2A) beyond which VORF data are not available, and conversion between ODN and CD is not possible. Beyond Stirling, a water level gradient is implemented through interpolation based on the water level indication at the upstream boundary (Craigforth station).

A spatially varying Manning roughness field is implemented after calibration (see Section 3.3). The time step is 10 s to satisfy the Courant-Friedrichs-Lewy criterion and secures sufficient computational efficiency. The model runs in parallel on a HPC server. Uniform horizontal eddy diffusivity and viscosity are considered and set to 0.1 m^2/s. The simulation period is from the 1st to 9th of December 2013, inclusive of storm Xaver (Table 2).

Table 2
Model input parameters.

Parameter	Value
Horizontal diffusion	0.1 m^2/s
Horizontal viscosity	0.1 m^2/s
Time step	10 s
Simulation period	01/12/2013 00:00:00–09/12/2013 23:45:00

3.3. Model calibration

The model is calibrated using observations from two stations in the Forth Estuary. Forth Ports Group, the Forth Estuary's ports operator and authority holds a database with historic datasets at the ports of Grangemouth and Rosyth (Fig. 2A). The calibration involves comparing water level time series for a spring tide period between the 6th and the 11th of February 2020. This period refers to another storm event (Ciara) of similar - but not higher - magnitude to the event under consideration. It is chosen for calibration because there were no data available at the two calibration stations before 2020.

Topographic surveys commissioned by Stirling Council provide Manning coefficients over 100 cross-sections between Craigforth and the port of Grangemouth. A spatially varying Manning roughness field is made by interpolating the coefficients onto the model grid upstream of Grangemouth while a uniform coefficient (0.03 $s/m^{1/3}$) is assumed initially downstream of it. The calibration is performed focusing on the high-water (HW) levels of the 10 tides within the simulation period. The root mean square error (RMSE) for HW levels at the Grangemouth and Rosyth stations is 0.15 m and 0.048 m respectively (Table 3). Williams and Esteves (2017) suggest the following calibration criteria for estuaries:

1) Tidal range differences less than 10 % of the spring tidal range
2) Water level differences less than 30 cm and 10 cm at the head and the mouth respectively

The resultant roughness field (Fig. 2B) leads to numerical results that satisfy the above criteria (see Table 3 and Fig. 3C, D).

3.4. Model validation

The model is validated using the roughness field given in Fig. 2B for a spring neap tide period in December 2020, which reached similar water levels as the February 2020 storm. We used to that end water levels at two stations. For the Grangemouth station, we use data over spring tides between 12 and 18 December 2020. For the Rosyth station the validation period starts 3 days later due to a gap in the data (Fig. 3E, F).

3.5. Fine model setup

The D-FLOW FM model is setup to accurately determine the hydrodynamics and flooding onset in the Forth estuary. A finer resolution model is set up around the study area to better understand the effects of vegetated land on flooding. Topographical features that are not resolved at coarse resolution can be important when vegetation is included as its effects are usually experienced at smaller scales. To force the model, timeseries of water levels (Fig. 4C) and an estuary flux (Fig. 4D) extracted from the coarse model are implemented at the downstream and upstream boundary respectively. The grid resolution can be as fine as 10 m in the river and coastal areas increasing gradually further inland to a maximum of 100 m (Fig. 4A). Bathymetric and topographic data are interpolated again in the D-FLOW FM fine grid by triangulation (Fig. 4B). The spatially varying roughness field is kept the same as in the coarse model. The fine resolution improves the representation of the topography. For instance, a relatively low altitude area is shown in Fig. 4B in white and greyish colour which does not exceed 2.5 m above ODN. Such features can be important since very often coastal flooding is limited by coastal topography (Huang, 2022).

3.5.1. Vegetation in the model

In D-FLOW FM, flow resistance from vegetated land can be parameterised through roughness classes also referred to as trachytopes (Deltares, 2021). Different roughness types can be defined at different locations in the computational domain. In this study, flow resistance due to vegetation is expressed through adaptations of analytical relationships for the bed shear stress on a vegetated bed as developed by Baptist (2005). These relationships consider flow resistance due to vegetation as cylindrical roughness and derive a Chezy coefficient with the following equation (Baptist, 2005):

$$C = \sqrt{\frac{1}{C_b^{-2} + \frac{C_D m D h_v}{2g}} + \frac{(h-h_v)^{3/2}\,\frac{\sqrt{g}}{\kappa}\,ln\left(\frac{h-h_v}{ez_0}\right)}{h^{3/2}}} \quad (1)$$

where, C_b the Chezy roughness for a non-vegetated bed, C_D a drag coefficient, m the number of stems per square meter, D the stems diameter, h_v the vegetation height, h the water depth, g the gravitational acceleration, κ the von Karman constant, z_0 the roughness length and e the base of the natural logarithm. Eq. (1) corresponds to the roughness due to submerged vegetation as long as $h_v \leq h$. When the vegetation height becomes equal to the water depth ($h = h_v$), the equation reduces to its first term on the right which expresses the flow resistance due to non-submerged vegetation.

Table 3
Statistical parameters after the calibration.

	Grangemouth	Rosyth
RMSE	0.15 m	0.048 m
Maximum HW difference	0.24 m	0.09 m
Mean tidal range difference	0.33 m	0.23 m

3.5.1.1. Vegetation model input and zones setup. In this study, we consider the development of vegetation zones seaward of Airth instead of MR. The target area (TA) can be divided in three separate sections (north, middle, south) by an unnamed watercourse and a road (Fig. 1B). Vegetation zones of various extents have been implemented in the model. The first scenario considers a vegetation zone that covers the entire TA. However, knowing that a change of land use over the entire TA would severely impact the local community's agricultural activities, alternative options have been investigated. Three separate scenarios are considered where vegetation covers only one section of the TA (north, middle or south). A special scenario has been set up where vegetation exists only between the coastline and approximately 100 m behind the embankment. Fig. 1B shows the extents of each vegetated area for every scenario. Table 5 lists all the scenarios and gives the size of the vegetation zone for each scenario.

To be realistic, the type of vegetation should correspond to the plant species that are present or able to grow in this area (*Puccinellia Maritima*, *Festuca Rubra* and *Jungus Gerurdii*). Coastal grasslands may show limited survival and growth when immersed into seawater after a flooding event (Hanley et al., 2016). We choose to only consider *Festuca Rubra* for our model simulations as it is known to have the best salt tolerance out of the three available species (Roy and Chakraborty, 2014). Input parameters for Eq. (1) have been determined based on information that can be found online for the traits of *Festuca Rubra*. It is noted that in the model, the existing salt marshes in front of the embankment and the vegetation on top of the embankment are also replaced by *Festuca Rubra*.

It is generally considered that increased vegetation height and density provide higher momentum absorption and reduce flows (e.g., Sheng et al., 2012; Baaij et al., 2021) and offer better protection against flooding. Therefore, the maximum height (80 cm) and stems diameter (3 mm) of *Festuca Rubra* that can be found in the UK (https://www.naturespot.org/) are implemented in each scenario. An indicative number of 1000 stems per m^2 is considered to represent a coverage as dense as possible (i.e. to assess the potential of established schemes). A shoot density of O (10^3) per m^2 is a good estimate based on literature (Bij De Vaate et al., 2020), lab experiments (Bouma et al., 2009, 2013) and field observations (Neumeier, 2007). The Chezy coefficient for the non-vegetated bed is taken equal to 65 $m^{1/2}/s$ following suggestions in the literature for the soil type in front of Airth (Best et al., 2018).

The drag coefficient is calculated separately for the north, middle and south sections using the equation by Sonnenwald et al. (2019):

$$C_D = 2\left(\frac{6475D + 32}{R_d} + 17D + 3.2\varphi + 0.50\right) \quad (2)$$

where R_D is the stems Reynolds given as $R_D = \frac{U_a D}{\nu}$, with U_a the flow velocity approaching the vegetation zone and ν the kinematic viscosity. The vegetation density φ (or otherwise referred to in the literature as the solid volume fraction) is equal to $\frac{m\pi D^2}{4}$. Eq. (2) is chosen because it has been tested and found successful against experimental data for low R_D which applies well in this case.

The flow velocity over each vegetation zone is a spatial and time average taken from the results of Scenario 1 where no vegetation is assumed. The same drag coefficients are used for Scenario 2 and Scenario 3 that include either all or parts of these three sections. The vegetation input parameters and the simulation period are kept the same in each scenario (Table 4 and Table 2). The full modelling approach is summarised and visualized in Fig. 5.

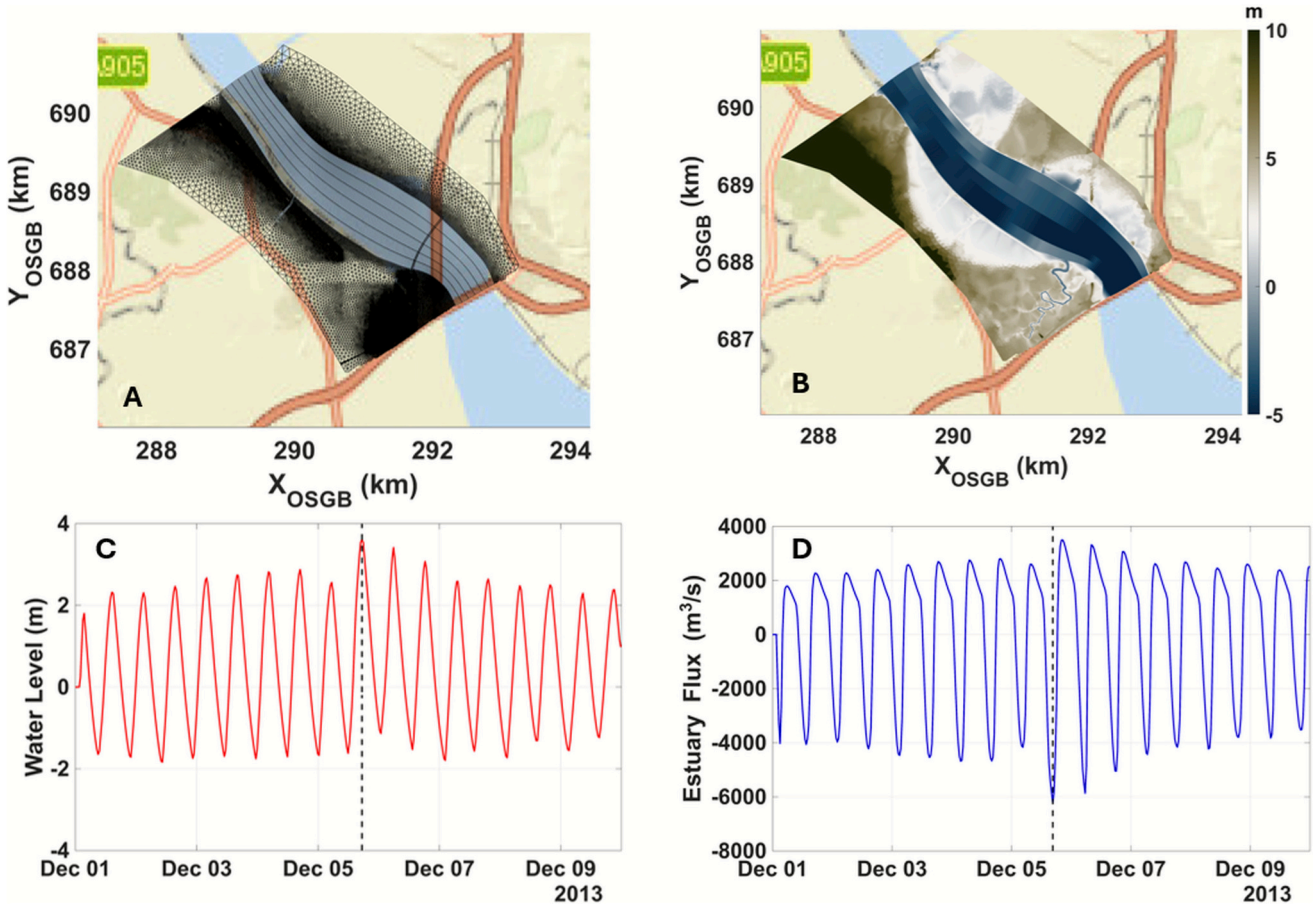

Fig. 4. Fine model A) Grid and B) Bathymetry. The depths are given with respect to the ODN (basemap: OpenStreets Map). The implemented time series of water level at the downstream (C) and the estuary flux at the upstream (D) boundaries. The black dashed vertical lines are drawn through the time of the maximum water level and flux observed during the simulation period.

4. Results

4.1. Water depths and flood extents

4.1.1. Reference scenario

The analysis of water depths and flood extents focuses only on the west side of the river where the case study (Airth) is located (Fig. 1B and C). Fig. 6A presents the water depths of the reference scenario at the time when the maximum high water (MHW) and estuary flux are implemented at the fine model boundaries (Fig. 4C). This occurs 3 h after the maximum water level was recorded at the Leith station (Fig. 3B). At the MHW, almost the entire TA (Fig. 1B) is flooded but the water depths vary between the three sections (north, middle and south). At the south and middle sections, the water depths vary between 2.5 m – 3 m just in front of the embankment and decrease gradually inland. Lower water depths can be observed at the north section that do not exceed 1.5 m. The flood extent in Fig. 6A roughly matches the TA. There are no satellite images depicting the flood extents at the peak of storm Xaver to compare with. However, these results have been communicated to the local authorities and community who qualitatively confirmed the validity of the model results.

Table 4
Vegetation input parameters in the model setup.

Vegetation parameter	Value
Stems diameter	0.003 m
Vegetation height	0.08 m
Stems density	1000 per m^2
Chezy coefficient	65 $m^{1/2}/s$
C_D (north section)	1.7
C_D (middle section)	1.58
C_D (South section)	1.47

4.1.2. Scenarios with vegetation and the current embankment

The results of the reference case (Scenario 1) are compared with those of the scenarios 2–6 where vegetation zones have been implemented between the river Forth and Airth. The comparison is done at the MHW time. Panels B–F of Fig. 6 show the water depth difference between the reference scenario and Scenarios 2–6. All the scenarios exhibit a local decrease of the water depths mainly in the north and middle sections. Scenario 2 (Fig. 6B), for which vegetation covers the entire TA, is the most effective one: vegetation induces a maximum decrease of 2 m in the middle section and 1 m in the north section. The effect is smaller when the vegetation is implemented only near the waterfront (Scenario 3, Fig. 6C) as water depths do not decrease by more than 1 m. A decrease in water depth by 1 m is also observed in Scenario 4 (Fig. 6D), but only within the limits of the north section where vegetation is included. Scenarios 5 and 6 (Fig. 6E and F respectively) show an expansion of vegetation's effect to adjacent areas. In all cases, the water depths in the south section do not change compared to the reference scenario. This is better illustrated in Fig. 7A that provides the flood extents for Scenarios 1–6. While the contour lines for each of the six scenarios are clearly separated in the north and middle sections, they all fall upon each other in the south section.

To understand the reason behind this, flow arrows are plotted on top of the bed level in Fig. 8. It is observed that in the reference scenario

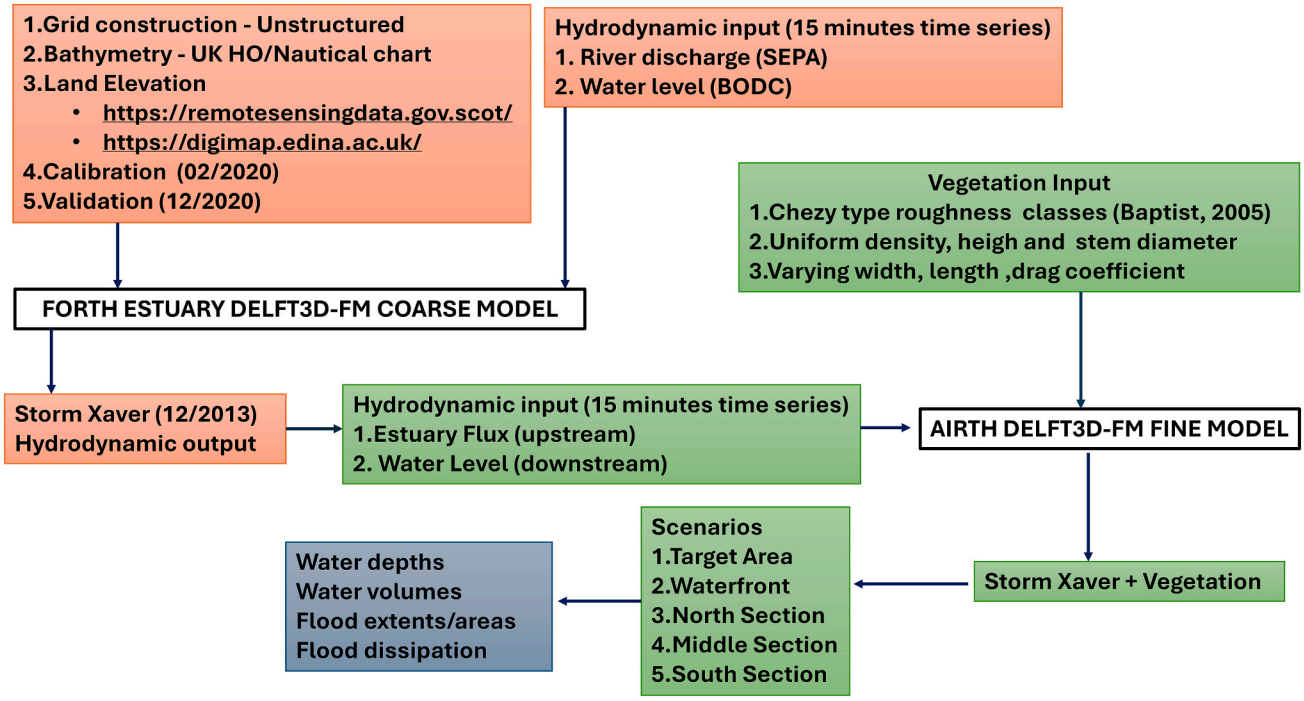

Fig. 5. Schematic diagram of the modelling approach and research framework.

(Fig. 8A), as the tide propagates inshore, a south to north current develops over the floodplain indicating that water primarily overtops the embankment at the south section, even though some overtopping does occur at the north section as well. This implies that the embankment may be lower at the south. Indeed, Fig. 8E discloses that the embankment can be as high as 5 m above OD at the north and middle sections while it does not exceed 2.5 m at the south section. As a result, the vegetation implemented in the TA (Fig. 8B) reduces only the flow velocity (smaller flow arrows) but not the water depths and cannot avert flooding at the south section. Figures depicting flow arrows for scenarios 3–6 and 9–12 can be found in the Supplementary (Fig. 1, Section 1.1 and Fig. 2, Section 1.2 respectively).

4.1.3. *Scenarios with vegetation and a raised embankment at the south section*

Fig. 6 indicates that the water depths in the south section do not differ from the reference scenario when vegetation is implemented. As discussed in Section 4.1.2, the difference in embankment height compromises the vegetation's effectiveness against flooding. Scenarios 1–6 are repeated with a different bathymetry such that the embankment at the south section is raised closer to the level of the two other sections (Fig. 8F). These simulations correspond to the Scenarios 7–12 listed in Table 5.

Fig. 9 shows the water depth difference between the reference scenario and Scenarios 7–12. Fig. 9A corresponds to Scenario 7 where the embankment is raised but no vegetation is added. Not surprisingly, a local increase of the embankment height causes a considerable decrease of the water depths especially in the middle and south sections. As seen in Fig. 8C, the raised embankment stops the south to north flow. The water overtops the embankment separately at the north and south sections and thus flooding is retained locally. This also offers protection to the middle section that does not get flooded and thus presents the maximum water depths difference (Fig. 9A). Scenarios 7 and 11 (Middle) exhibit almost identical results (Fig. 9A and E respectively), which suggests that adding vegetation is not needed to protect the middle section in this case. Almost identical results are also observed between the TA (#8) and the Waterfront (#9) scenarios (Fig. 9B and C respectively), which are the most effective scenarios providing both maximum decrease of 3 m in water depths and minimum flood extents (Fig. 7B). Since the vegetation cover in the Waterfront scenarios (#3 and #9) is about 5 times smaller in size than that of the TA scenarios (#2 and #8), this suggests that equivalent flood protection could be attained while incurring substantially less land loss.

Fig. 9 demonstrates that the combination of a raised embankment and vegetation introduced in the various sections has an impact throughout the entire site in all cases and offers much better protection compared to the results in Section 4.1.2 (Fig. 6). Fig. 8D indicates that adding vegetation does not change the flow pattern compared with Fig. 8C but further decreases the flow magnitude and flood extents. Water is trapped in the north section (Fig. 8C and D) and is only reduced in depth when vegetation is present in this section, which is the case in Scenario 8, 9 and 10 (Fig. 9 B, C and D respectively). If there is no vegetation in the north section, flooding cannot be averted as is the case in Scenarios 7, 11 and 12 (Fig. 9 A, E and F respectively). On the contrary, flood impact at the south section is reduced irrespective of any vegetation because of the higher embankment. For the south section, despite the water depths decrease observed in all scenarios, the flooded area extents are only reduced in the three scenarios that include vegetation in the south section. As depicted in Fig. 7B, the South (#12), Waterfront (#9) and TA (#8) scenarios (magenta, blue and red contours respectively) flood an equal area which is much smaller than that of the three other scenarios. These results underscore the critical role of vegetation field position in relation to the prevalent flow paths.

4.2. *Flood dissipation potential per scenario*

In Scenarios 2–11, interventions are implemented in the form of either a vegetation zone or vegetation plus embankment. The effect of these interventions can be quantified for each scenario through the following equation that expresses the flood dissipation as the percentage decrease of the water volume compared with the reference scenario:

$$DP = 1 - \frac{\sum_{i=1}^{n} H_i dxdy}{\sum_{i=1}^{n} H_0 dxdy} \quad (3)$$

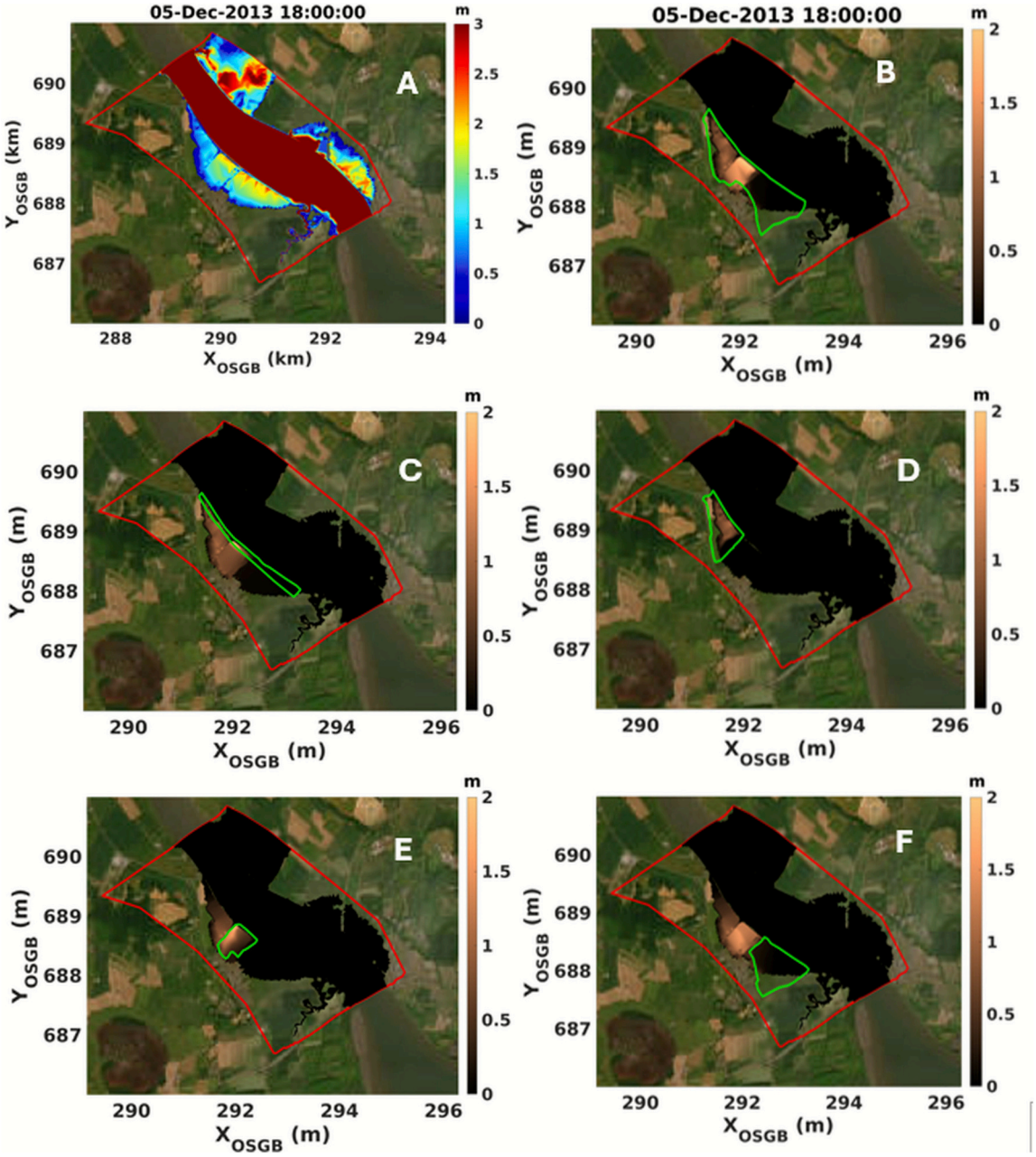

Fig. 6. A) The water depths at the reference scenario at the peak of the storm. B), C), D), E), F) The water depth decrease compared to the reference scenario (Scenario 1) caused by the vegetation in the TA (Scenario 2), Waterfront (Scenario 3), North (Scenario 4), Middle (Scenario 5) and South (Scenario 6) scenarios respectively. The red line delineates the fine resolution model borders. The green polygons enclose the vegetated zone in each scenario. The results correspond to the simulations with the current embankment. (basemap: Google Earth).

Where H the maximum water depth in a grid cell i with dx and dy its horizontal dimensions. The subscripts I and o indicate the presence and the absence of interventions respectively. Eq. (3) is an adaptation of the equation given by Sheng et al. (2012) to measure the vegetation dissipation potential. However, in this study, DP accounts for the effect of any intervention type (vegetation or vegetation plus embankment) and not just vegetation. As in Section 4.1, the DP is calculated at the MHW time at the fine model boundary and incorporates the changes in both water depths and flood extents at each time. In Fig. 10, the DP is given in the form of a bar chart against the vegetated zone (measured in hectares) of each scenario for the case of the current embankment (blue bars) and that of the raised one (orange bars).

For the current embankment simulations (blue bars in Fig. 10), the flow resistance from vegetation is maximum for scenario 2 (TA) where a DP of 50 % is achieved. Implementing vegetation over the entire TA can be very effective even without raising the embankment. The Waterfront (#3) and South (#6) scenarios present equal results and 42 % DP. Given the respective converted areas for each scenario, the Waterfront scenario offers the highest flood dissipation per hectare. The high efficiency of these three scenarios can be ascribed to the inclusion of vegetation in the south section which prevents the current flow from the south to the north of the TA (Fig. 8A). This highlights how important it is to consider the flow direction and pathways when deciding where to implement vegetation. In fact, the results show a deterioration of the DP with the distance from the south section as the Middle one (#5) provides 36 % dissipation and the North (#4) only 7 % being the most distant case from the source of the prevalent flow path.

Not surprisingly, when the embankment is raised at the south

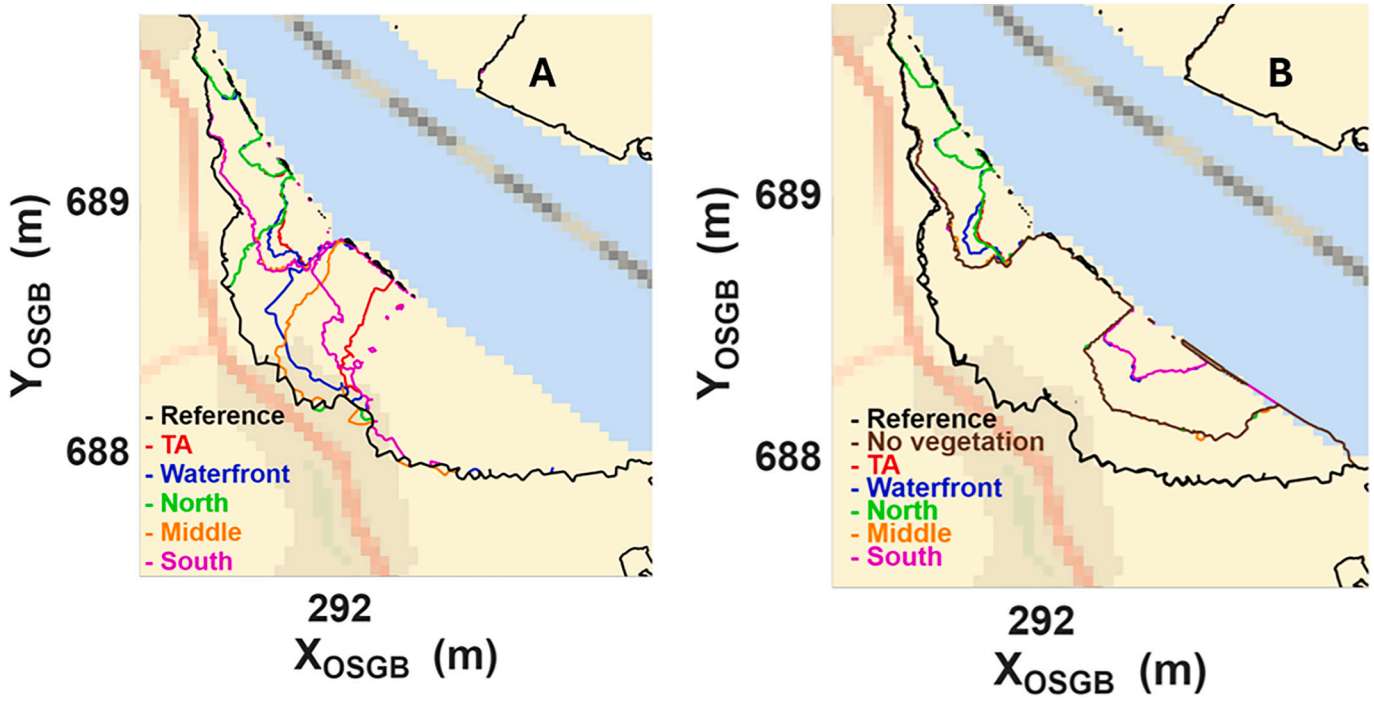

Fig. 7. The maximum flood extents for A) scenarios 1–6 and B) scenarios 7–12. (basemap: Open Streets map).

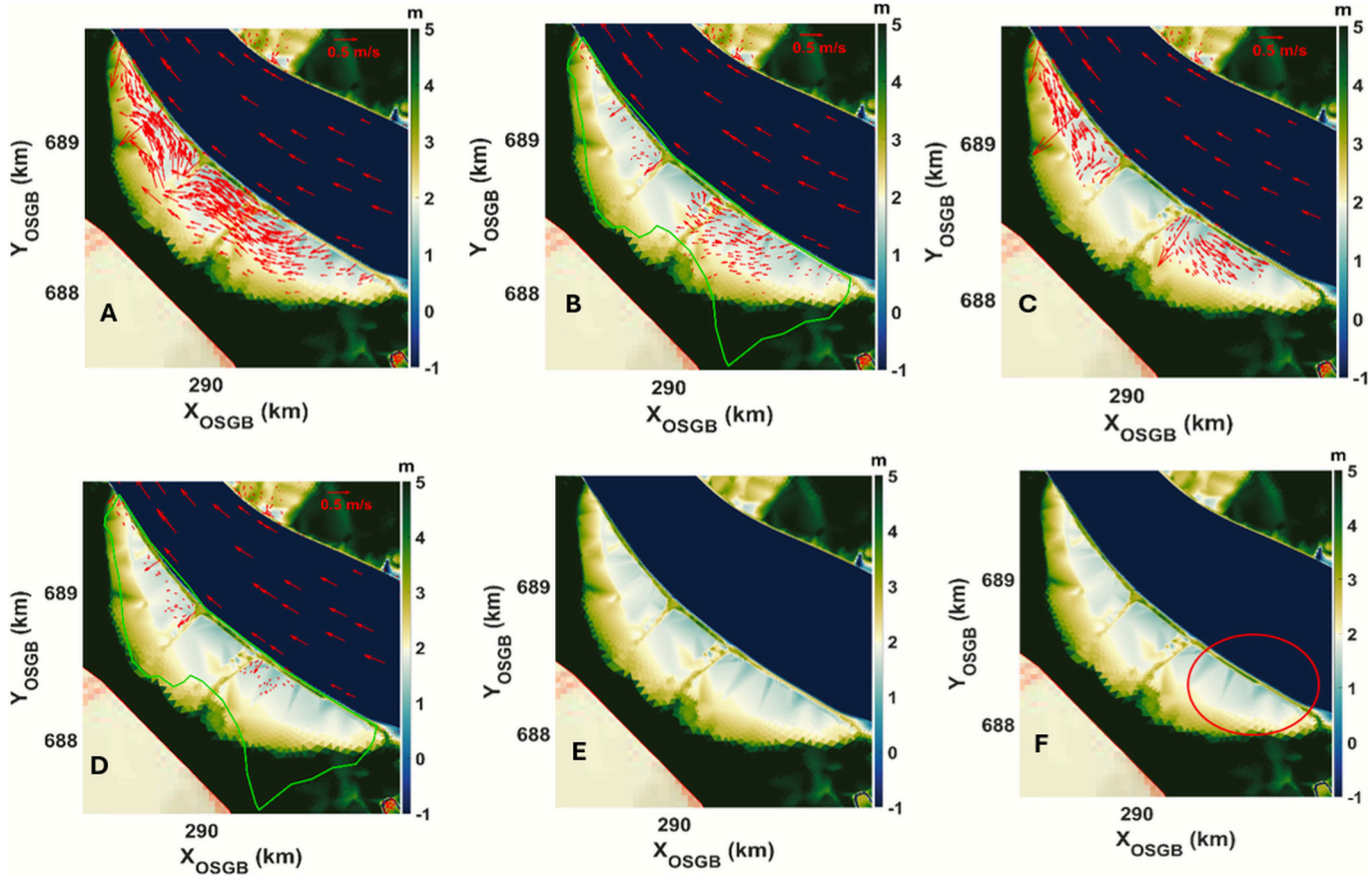

Fig. 8. Flow arrows on top of bed levels at the MHW for A) Scenario 1 (reference), B) Scenario 2 (vegetation in the entire TA), C) Scenario 7 (raised embankment but no vegetation and D) Scenario 8 (raised embankment with vegetation in the entire TA). E), F). Bed level (m above OD) showing the land elevation with the current (scenarios 1–6) and raised embankment (scenarios 7–12) respectively. Panel E clearly shows a much lower elevation at the south section. Panel F shows an increased land elevation along the south section of the embankment encircled by a red line circle.

Table 5
The list of simulations executed and the area in ha, maximum across-shore (width) and along-shore (length) distances of the vegetated field in each case. Scenario 1 is the reference case where no vegetation is considered. Scenario 3 under the name Waterfront considers vegetation to be between the coastline and up to 100 m behind the embankment. All the simulations are repeated with the same setup but a higher embankment (see Section 4.1) and is assigned the number inside the parenthesis in the first column.

Scenario	Vegetated zone	Area (ha)	Width (m)	Length (m)
1 (7)	–	–	–	–
2 (8)	Target area	155	1000	2500
3 (9)	Waterfront	32	200	2500
4 (10)	North section	48	750	1100
5 (11)	Middle section	27	650	400
6 (12)	South section	69	1000	1000

section, the DP significantly increases for every scenario and varies between 80 % and 92 %. The most interesting outcome is that Waterfront (#9) and TA (#8) show an equal dissipation of 92 %. Raising the embankment offers higher protection and could require less land converted to achieve equally high dissipation. The DP equality between the North (#10) and South (#12) scenarios is also important, not only because of the high flood dissipation values (85 %) but because it demonstrates the impact of changes to the flow path regarding the vegetation efficiency. As discussed in Section 4.1.3, Fig. 8C indicates that there is no flow exchange between the south and north areas when the embankment is raised at the south section. Consequently, the effect of vegetation from the north section is higher and leads to a very large increase of this scenario's DP from 7 % to 85 %. Scenario 7 (raised embankment but no vegetation) and 11 (Middle, raised embankment) present equal DP because the middle section does not get flooded (Fig. 8C).

5. Discussion

5.1. Controlling factors of vegetation effectiveness against flooding

The findings in Section 4 provide insights that facilitate the determination of critical parameters affecting vegetation's effectiveness against flooding and ultimately design criteria for any mitigation scheme. Table 5 displays the maximum across and along shore distances (i.e., width and length respectively) of the five vegetation zones that have been considered in the simulations. Even though the maximum width is less or equal to 1 km in all scenarios, the results in Fig. 6 and Fig. 9 show a significant decrease in water depths for most cases. The same applies for the flood extents, seen in Fig. 7A and B. It is inferred that the decrease is caused by both the increase in friction due to vegetation and the effect of the embankment that stops overtopping. Fig. 10 and Table 6 do not show any trend between dissipation potential and the size of the vegetation zone, only that the best results are obtained for Scenarios 2 and 8 (TA) where the maximum vegetated area is implemented (155 ha). Kiesel et al. (2022) assessed the effectiveness of the MR site at Freiston Shore (UK) which encompasses 66 ha, one of the largest schemes in Europe, and argued that sites of smaller or even equal size usually provide limited protection. Notably, except for the TA and South scenarios, the vegetation zones considered here are less than 66 ha. Nevertheless, all of them result in a considerable flood reduction as demonstrated in Fig. 10. This must be attributed to the presence of the embankment which enhances the dissipation potential in all cases. Kiesel et al. (2022) also observed the effect of reflection in front of the breached dike at Freiston Shore which resulted in higher attenuation and the demand of lower landward sea wall specifications.

Interestingly, Fig. 10 indicates that the TA and Waterfront scenarios present the maximum flood dissipation while the converted land in the latter case is about 5 times smaller than that of the former. In addition, the across-shore distance between the river and the end of the vegetation patch is also 5 times smaller in the Waterfront case. This is an indication that at small widths (< 1 km) and in the presence of hard engineering solutions, the length of the vegetated zone might be more important than the width. The longitudinal extent of the vegetation patch is about 2.5 km in both cases (Table 5). The third best case regarding dissipation potential, is the South scenario in the simulations with the current embankment (#6) but the North scenario becomes more favourable with the raised embankment (#10). The length of the South and North vegetation zones is comparable (1 km and 1.1 km respectively), which implies the presence of another factor determining the efficiency of each intervention. Fig. 8A indicates the existence of a south to north current flow when the current embankment is considered so that the water enters the TA from the south and flows to the north. If the vegetation is implemented only at the north section, then the south to north current flow is left unaffected and the flow circulation is the same as that of the reference scenario (#1). The South scenario (#6) is considered preferable because the vegetation is placed closer to the flow source and interferes with the main flow path. On the contrary, the results are reversed when the embankment is raised because the south to north current flow disappears (Supplementary, Fig. 2B and D). In this case, the South scenario (#12) is less effective than the North (#10) because its effect is limited locally and has no influence on flooding at the north and middle sections. This points to the fact, that the effect of interventions including vegetation zones, does not solely depend on their dimensions but also to their position relative to the prevalent flow circulation. Therefore, it is important for coastal managers to consider the changes that the implementation of a vegetated zone will cause to the flow paths before assessing the potential benefits of an intervention.

5.2. Significance of results

By examining the flood mitigation of a hybrid defence comprising an embankment and vegetation zones against storm Xaver, this study provides quantitative evidence that shows hybrid defences are more effective than fully natural solutions at attenuating storm surge flooding (e.g. Taylor-Burns et al., 2025; Lathrop et al., 2019). In our case study, adding vegetation in front, on top and behind of an embankment reduced the storm's floodwater volume by up to 50 % (Fig. 10). Yet, the presence of the embankment is critical and improving it leads to significantly better protection (Fig. 10). A MR scheme may over time enable the establishment of an intertidal habitat seaward of Airth. However, Airth is less than 1 km from the estuary with some houses only 500 m from the shore, so effective mitigation of coastal flooding would still be highly uncertain given the limited space available.

Space is an important consideration for coastal management (e.g. Villasante et al., 2023). For example, lack of accommodation space is a common and key limiting factor for vegetations' effectiveness against storm surge impact (Taylor-Burns et al., 2025; Du et al., 2020; Chen et al., 2024; Bouma et al., 2014; Lathrop et al., 2019). Within the context of competing uses of coastal space, the maximum modelled flood reduction in our results was provided by two scenarios (#8 and #9, TA and Waterfront respectively) with very different land use (Table 4 and Fig. 10). This suggests that the maximum flood reduction could be achieved without extensive land conversion. Coastal communities may be more inclined to endorse solutions requiring limited land conversion.

Pressures on coastal space can arise due to several factors including the geomorphology of the coastal landscape, the presence of urban areas, and coastal squeeze. In our case study, the primary pressure is land use. Habitat restoration is often opposed by farmers who are unwilling to relinquish their land (Apine and Stojanovic, 2024). This challenge is widespread across most of the world's estuaries and deltas, where extensive wetlands have been lost through land reclamation (Smolders et al., 2015; Schuerch et al., 2022) and converted into productive agricultural land. These zones remain low-lying and highly vulnerable to flooding (Schuerch et al., 2022). The inner Forth Estuary, where Airth is located, is a typical example: more than 50 % of its former

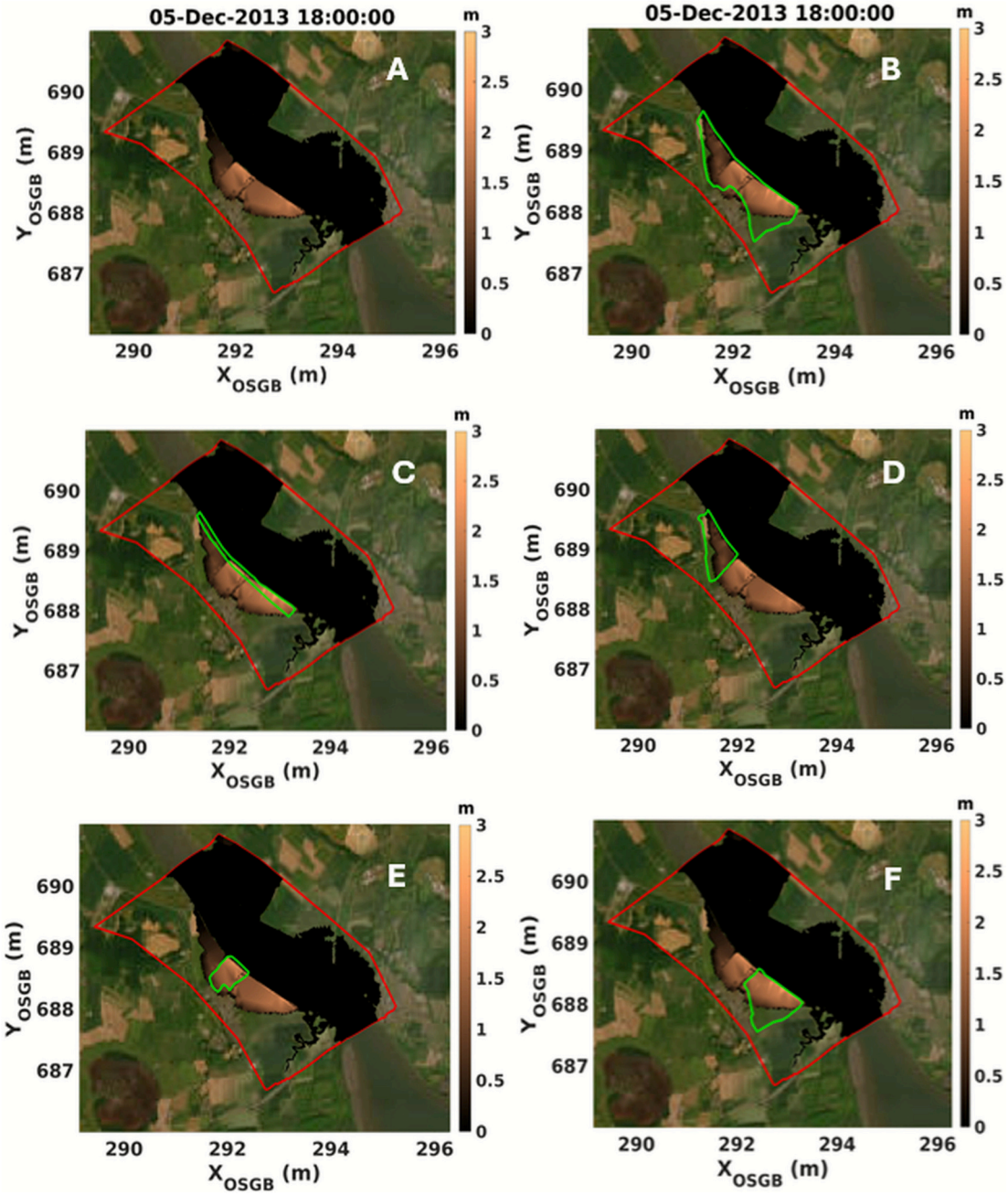

Fig. 9. A) The water depths decrease caused by simply raising the embankment at the south without any vegetation added (Scenario 7). B), C), D), E), F). The water depths decrease caused by raising the embankment at the south and adding vegetation at the TA (Scenario 8), Waterfront (Scenario 9), North (Scenario 10), Middle (Scenario 11) and South (Scenario 12) scenarios respectively. The red line delineates the fine resolution model borders. The green polygons enclose the vegetated zone in each scenario. The results correspond to the simulations with the raised embankment. (basemap: Google Earth).

intertidal habitats have been lost to land reclamation (Liski et al., 2019). In many coastal communities, agriculture is the primary source of income and surrendering farmland can have severe socio-economic consequences. Our modelling suggests that careful design of a hybrid coastal protection scheme can combine flood protection with preserving the livelihood of the local community.

Furthermore, over two-thirds of the coastal population are estimated to live in small settlements (Fitton et al., 2020). Adaptation to climate change impacts, such as increased risk of flooding, differs between small rural and larger urban communities (Lehmann et al., 2021). The evidence presented here for Airth, and the inner Forth Estuary focuses on relatively small rural community representative of a broader range of small agricultural coastal communities, which are often overlooked in academic literature on coastal management solutions (e.g. Mortensen et al., 2024). A significant challenge for smaller settlements is the lack of reliable data on coastal flooding, either because these are not included in regional and national reports and/or state-of-the-art data collection methods are inaccessible to these communities (Lehmann et al., 2021). In this context, engagement with residents becomes essential, as they often hold valuable knowledge and information of past storm events and their impact. Such an approach has been central in the present study where the methodology has been largely developed after engagement with the Airth community through delivery of workshops and resilience-building events.

Although these results may not be directly transferable to other case studies -owing to limitations related to vegetation characteristics (see

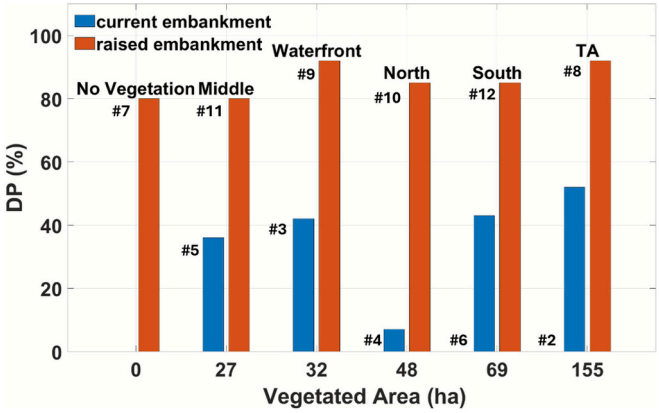

Fig. 10. Bar chart illustrating the dissipation potential against the vegetated area for Scenario 2–12. Scenario numbers are indicated by a hash on the left of each bar.

Table 6
The area in hectares of each vegetation zone in every scenario and the maximum inundated area in each case.

Scenario	Vegetated zone (ha)	Inundated area (ha)
1	–	126
2	155	66
3	32	95
4	48	102
5	27	107
6	69	110
7	–	80
8	155	30
9	32	35
10	48	59
11	27	80
12	69	52

Section 5.3) and/or variations in embankment height- they offer valuable insights that can inform other cases with comparable settings and challenges.

5.3. Limitations

5.3.1. Seasonality

Vegetated bed flow resistance might not be constant throughout the year. During wintertime, vegetation (i.e., density, height and diameter) can decrease and thus bed roughness reduce (Baaij et al., 2021). The selected plant in the simulations (*Festuca Rubra*) is a perennial plant meaning that it is expected to die out during the autumn and winter and grow back in the spring from its rootstock. Storm Xaver occurred in December when the *Festuca Rubra* biomass would be reduced.

However, the biomass loss in perennial plants is much smaller than in annual species (Baaij et al., 2021). They keep their below-ground root system during winter and so, even though diminished, flow resistance still exists and the bed might be stabilised at a higher elevation through sediment trapping (Silinski et al., 2016). Even though the timing of storm Xaver may result in an overestimation of the effect of vegetation, any seasonality effect on the results is not expected to have significant -at least qualitatively- influence because of the characteristics of the implemented vegetation.

5.3.2. Flexibility/rigidness

In Baptist's method (Eq. (1)), the vegetation is assumed to be in the form of rigid cylindrical elements. This approach has been widely adopted in many modelling studies with very good results (e.g., Best et al., 2018; Bij De Vaate et al., 2020). There is a concern though that representing vegetation as cylinders might be inaccurate regarding geometrical and mechanical properties of the vegetation stems (Garzon et al., 2019). In reality, flexible stems bend from higher flow velocities and their resistance to flow decreases because part of them becomes aligned to the flow direction (Garzon et al., 2019). Vargas-Luna et al. (2016) reviewed results from numerical model simulations and compared them with flume experiments using both plastic and real plants. They discovered a sensitivity of the Baptist method to the bare soil Chezy coefficient which might result in an underestimation of water depths especially in rough beds. On the other hand, they found better agreement between model results (using Baptist's method) and lab experiments for high-density grass and herbaceous vegetation which applies to the current study.

5.4. Sensitivity to vegetation density changes

All the investigated scenarios were performed assuming a constant vegetation height (0.8 m) and density (1000 stems/m^2). The maximum height of *Festuca Rubra* was selected to represent conditions of maximum dissipation. The vegetation drag coefficient and thus flow resistance generally increase with vegetation density. In absence of field data, we adopted an indicative but relatively high density for our modelling scenarios. We carried out two additional simulations to investigate the sensitivity of our results to vegetation density. To disentangle density effects from those associated with vegetation zone size or embankment height, the analysis was restricted to Scenario 2 (TA). This scenario includes the most extensive vegetation zone and yields the greatest flood dissipation. Scenario 2 is repeated with a 50 % decrease and increase of density. The results of these simulations are available in the Supplementary Materials (Section 2, Fig. 3 and Fig. 4).

As expected, a 50 % decrease of the vegetation density led to smaller reductions on water depths (S2, Fig. 3) and a decrease of the dissipation potential from 52 % in Scenario 2 to 35 % (S2, Fig. 4). A 50 % increase of the vegetation density did not cause further decreases of the water depth compared to the original Scenario 2 (S2, Fig. 3C) and resulted in a lower dissipation potential (42 %). This can be attributed to the blockage effect (Etminan et al.,2017; Liu and Wang, 2024), whereby an increase of vegetation stems reduces the flow cross-sectional area causing an increase of flow velocity across the vegetation zone (Liu and Wang, 2024). This reduces the wake pressure behind the stems (Etminan et al., 2017) which might explain the slightly higher water depths observed relative to Scenario 2. This may suggest the existence of a density threshold, beyond which an increase of vegetation density cannot enhance anymore the vegetation's flood dissipation capacity.

6. Conclusions

Delft3D-FM is implemented to investigate the effectiveness of a hybrid defence on local storm attenuation. The village of Airth, situated in the inner Forth estuary (Scotland, UK) is used as a case study. The hybrid defence consists of an embankment and vegetation zones at various locations seaward of the village. Five vegetation scenarios were setup and compared with a 'no vegetation' scenario using conditions during storm Xaver (December 2013). The simulations were repeated with the same vegetation zones but with a raised embankment. The main conclusion was that in the presence of an embankment, the alongshore extent of a vegetation zone might be more important than the across-shore extent. The implication is that a hybrid defence can reduce agricultural land loss, potentially reducing social resistance and concerns from local communities. The model results indicate that the vegetation's efficiency can be affected by its position and orientation relative to the prevalent flow paths. As such a good understanding of flow paths is needed for the design of such solutions. The present study provides useful conclusions for coastal managers and practitioners on the use and benefits of hybrid defences particularly in low space areas but there will need to be further tested in other study cases as well. Future research could also expand from flood protection to consider

other ecosystem services (e.g., carbon sequestration, biodiversity enhancement) that hybrid defences might offer.

CRediT authorship contribution statement

Constantinos Matsoukis: Visualization, Validation, Software, Methodology, Investigation, Formal analysis, Data curation, Conceptualization, Writing – review & editing, Writing – original draft. **Marta Payo Payo:** Supervision, Methodology, Conceptualization, Writing – review & editing. **Jennifer Brown:** Supervision, Project administration, Methodology, Conceptualization, Writing – review & editing. **Laurent Amoudry:** Supervision, Project administration, Funding acquisition, Conceptualization, Writing – review & editing.

Funding sources

This work was supported by the Co-Opt project (NE/V016423/1) funded by UK Research and Innovation (UKRI) via the Sustainable Management of UK Marine Resources (SMMR) Strategic Priorities Fund.

Declaration of competing interest

The authors declare that they have no known competing financial interests or personal relationships that could have appeared to influence the work reported in this paper.

Acknowledgements

The authors gratefully acknowledge the support provided by Forth Ports Group, UK Hydrographic Office, British Oceanographic Data Centre and Stirling Council in supplying data essential to this research, for model setup, calibration, datum conversion and topographical survey information including Manning coefficients. We also extend our appreciation to the Co-Opt team, and especially to Marta Meschini from the University of Liverpool, Sara Kaffashi from the Cranfield University, Elina Apine from the University of St Andrews, and Amani Becker from the National Oceanography Centre for their valuable contributions and assistance throughout various stages of the project.

Appendix A. Supplementary data

Supplementary data to this article can be found online at https://doi.org/10.1016/j.scitotenv.2025.181063.

Data Availability

Model output files are accessible in Zenodo DOI: https://doi.org/10.5281/zenodo.15861994.

References

Apine, E., Stojanovic, T., 2024. Is the coastal future green, grey or hybrid? Diverse perspectives on coastal flood risk management and adaptation in the UK. Camb. Prisms Coast. Futur. 2, e4. https://doi.org/10.1017/cft.2024.4.

Areia, N.P., Tavares, A.O., Costa, P.J.M., 2023. Public perception and preferences for coastal risk management: evidence from a convergent parallel mixed-methods study. Sci. Total Environ. 882, 163440. https://doi.org/10.1016/j.scitotenv.2023.163440.

Austin, W., Smeaton, C., Houston, A., Balke, T., 2022. Scottish Saltmarsh, Sea-Level Rise, and the Potential for Managed Realignment to Deliver Blue Carbon Gains. https://doi.org/10.7488/ERA/2370.

Baaij, B.M., Kooijman, J., Limpens, J., Marijnissen, R.J.C., Van Loon-Steensma, J.M., 2021. Monitoring impact of salt-marsh vegetation characteristics on sedimentation: an outlook for nature-based flood protection. Wetlands 41, 76. https://doi.org/10.1007/s13157-021-01467-w.

Baptist, M.J., 2005. Modelling Floodplain Biogeomorphology. Ph.D. thesis,. Delft University of Technology.

Best, Ü.S.N., Van Der Wegen, M., Dijkstra, J., Willemsen, P.W.J.M., Borsje, B.W., Roelvink, D.J.A., 2018. Do salt marshes survive sea level rise? Modelling wave action, morphodynamics and vegetation dynamics. Environ. Model. Softw. 109, 152–166. https://doi.org/10.1016/j.envsoft.2018.08.004.

Bij De Vaate, I., Brückner, M.Z.M., Kleinhans, M.G., Schwarz, C., 2020. On the impact of salt marsh pioneer species-assemblages on the emergence of intertidal channel networks. Water Resour. Res. 56, e2019WR025942. https://doi.org/10.1029/2019WR025942.

Bomers, A., Schielen, R.M.J., Hulscher, S.J.M.H., 2019. The influence of grid shape and grid size on hydraulic river modelling performance. Environ. Fluid Mech. 19, 1273–1294. https://doi.org/10.1007/s10652-019-09670-4.

Bouma, T.J., Friedrichs, M., Van Wesenbeeck, B.K., Temmerman, S., Graf, G., Herman, P. M.J., 2009. Density-dependent linkage of scale-dependent feedbacks: a flume study on the intertidal macrophyte *Spartina anglica*. Oikos 118, 260–268. https://doi.org/10.1111/j.1600-0706.2008.16892.x.

Bouma, T.J., Temmerman, S., Van Duren, L.A., Martini, E., Vandenbruwaene, W., Callaghan, D.P., Balke, T., Biermans, G., Klaassen, P.C., Van Steeg, P., Dekker, F., Van De Koppel, J., De Vries, M.B., Herman, P.M.J., 2013. Organism traits determine the strength of scale-dependent bio-geomorphic feedbacks: a flume study on three intertidal plant species. Geomorphology 180–181, 57–65. https://doi.org/10.1016/j.geomorph.2012.09.005.

Bouma, T.J., Van Belzen, J., Balke, T., Zhu, Z., Airoldi, L., Blight, A.J., Davies, A.J., Galvan, C., Hawkins, S.J., Hoggart, S.P.G., Lara, J.L., Losada, I.J., Maza, M., Ondiviela, B., Skov, M.W., Strain, E.M., Thompson, R.C., Yang, S., Zanuttigh, B., Zhang, L., Herman, P.M.J., 2014. Identifying knowledge gaps hampering application of intertidal habitats in coastal protection: opportunities & steps to take. Coast. Eng. 87, 147–157. https://doi.org/10.1016/j.coastaleng.2013.11.014.

Chen, Q., Li, Y., Kelly, D.M., Zhang, K., Zachry, B., Rhome, J., 2021. Improved modeling of the role of mangroves in storm surge attenuation. Estuar. Coast. Shelf Sci. 260, 107515. https://doi.org/10.1016/j.ecss.2021.107515.

Chen, Z., Luo, F., Zhou, G., Zhu, F., Wu, H., Li, R., Zhang, C., 2024. Hydrodynamic modeling study of nature-based hybrid coastal defense strategy applied in salt marsh restoration. Estuar. Coast. Shelf Sci. 298, 108666. https://doi.org/10.1016/j.ecss.2024.108666.

Christakos, K., Cheliotis, I., Varlas, G., Steeneveld, G.-J., 2016. Offshore wind energy analysis of cyclone Xaver over North Europe. Energy Procedia 94, 37–44. https://doi.org/10.1016/j.egypro.2016.09.187.

De Dominicis, M., Wolf, J., Jevrejeva, S., Zheng, P., Hu, Z., 2020. Future interactions between sea level rise, tides, and storm surges in the world's largest urban area. Geophys. Res. Lett. 47, e2020GL087002. https://doi.org/10.1029/2020GL087002.

Deltares, 2021. D-FLOW Flexible Mesh, Computational Cores and User Interface, User Manual. v0.9.1. Deltares, Netherlands.

Du, S., Scussolini, P., Ward, P.J., Zhang, M., Wen, J., Wang, L., Koks, E., Diaz-Loaiza, A., Gao, J., Ke, Q., Aerts, J.C.J.H., 2020. Hard or soft flood adaptation? Advantages of a hybrid strategy for Shanghai. Glob. Environ. Chang. 61, 102037. https://doi.org/10.1016/j.gloenvcha.2020.102037.

Environment Agency, 2018. Coastal Flood Boundary Conditions for the UK: Update 2018. Technical Summary Report. https://assets.publishing.service.gov.uk/media/5d667084e5274a170c435326/Coastal_flood_boundary_conditions_for_the_UK_2018_update_-_technical_report.pdf.

Etminan, V., Lowe, R.J., Ghisalberti, M., 2017. A new model for predicting the drag exerted by vegetation canopies. Water Resour. Res. 53, 3179–3196. https://doi.org/10.1002/2016WR020090.

Fitton, James, Lehmann, Martin, Major, David C., 2020. Identifying coastal towns and small cities in Denmark using global population data to support climate change adaptation. 0Int. J. Digital Earth 13 (9), 1040–1054. https://doi.org/10.1080/17538947.2019.1642403.

Garzon, J.L., Maza, M., Ferreira, C.M., Lara, J.L., Losada, I.J., 2019. Wave attenuation by *Spartina* saltmarshes in the Chesapeake Bay under storm surge conditions. J. Geophys. Res. Oceans 124, 5220–5243. https://doi.org/10.1029/2018JC014865.

Gedan, K.B., Kirwan, M.L., Wolanski, E., Barbier, E.B., Silliman, B.R., 2011. The present and future role of coastal wetland vegetation in protecting shorelines: answering recent challenges to the paradigm. Clim. Chang. 106, 7–29. https://doi.org/10.1007/s10584-010-0003-7.

Haigh, I.D., Ozsoy, O., Wadey, M.P., Nicholls, R.J., Gallop, S.L., Wahl, T., Brown, J.M., 2017. An improved database of coastal flooding in the United Kingdom from 1915 to 2016. Sci. Data 4, 170100. https://doi.org/10.1038/sdata.2017.100.

Hanley, M.E., Gove, T.L., Cawthray, G.R., Colmer, T.D., 2016. Differential responses of three coastal grassland species to seawater flooding. J. Plant Ecol., rtw037 https://doi.org/10.1093/jpe/rtw037.

He, J.Y., Lau, T.K., Chan, Y.W., Cheung, P., Lam, C.C., Choy, C.W., Chan, P.W., 2025. An observational analysis of Super Typhoon Yagi (2024) over the South China Sea. Meteorol. Atmospheric Phys. 137. https://doi.org/10.1007/s00703-025-01069-9.

Huang, P.-C., 2022. An effective alternative for predicting coastal floodplain inundation by considering rainfall, storm surge, and downstream topographic characteristics. J. Hydrol. 607, 127544. https://doi.org/10.1016/j.jhydrol.2022.127544.

Justine, Y.E.D., Seenath, A., 2025a. Modelling the effectiveness of vegetative nature-based solutions for coastal flood risk mitigation. J. Flood Risk Manag. 18, e70046. https://doi.org/10.1111/jfr3.70046.

Justine, Y.E.D., Seenath, A., 2025b. Vegetative nature-based solutions for coastal flood risk management: benefits, challenges, and uncertainties. Ocean Coast. Manag. 261, 107520. https://doi.org/10.1016/j.ocecoaman.2024.107520.

Kettle, A.J., 2020. Storm Xaver over Europe in December 2013: overview of energy impacts and North Sea events. Adv. Geosci. 54, 137–147. https://doi.org/10.5194/adgeo-54-137-2020.

Kiesel, J., MacPherson, L.R., Schuerch, M., Vafeidis, A.T., 2022. Can managed realignment buffer extreme surges? The relationship between marsh width, vegetation cover and surge attenuation. Estuar. Coasts 45, 345–362. https://doi.org/10.1007/s12237-021-00984-5.

Lathrop, R.G., Irving, W., Seneca, J.J., Trimble, J., Sacatelli, R.M., 2019. The limited role salt marshes may have in buffering extreme storm surge events: case study on the New Jersey shore. Ocean Coast. Manag. 178, 104803. https://doi.org/10.1016/j.ocecoaman.2019.05.005.

Lee, W., Sun, A.Y., Scanlon, B.R., Dawson, C., 2024. Hindcasting compound pluvial, fluvial and coastal flooding during Hurricane Harvey (2017) using Delft3D-FM. Nat. Hazards 120, 851–880. https://doi.org/10.1007/s11069-023-06247-9.

Lehmann, M., Major, D.C., Fitton, J., Doust, K., O'Donoghue, S., 2021. The way forward: supporting climate adaptation in coastal towns and small cities. Ocean Coast. Manag. 212, 105785. https://doi.org/10.1016/j.ocecoaman.2021.105785.

Leonardi, N., Carnacina, I., Donatelli, C., Ganju, N.K., Plater, A.J., Schuerch, M., Temmerman, S., 2018. Dynamic interactions between coastal storms and salt marshes: a review. Geomorphology 301, 92–107. https://doi.org/10.1016/j.geomorph.2017.11.001.

Liski, A.H., Ambros, P., Metzger, M.J., Nicholas, K.A., Meriwether, A., Wilson, W., Krause, T., 2019. Governance and stakeholder perspectives of managed re-alignment: adapting to sea level rise in the inner forth estuary, Scotland. Reg. Environ. Chang. 19, 2231–2243. https://doi.org/10.1007/s10113-019-01505-8.

Liu, Y., Wang, P., 2024. Drag in vegetation canopy: considering sheltering and blockage effects. Water Resour. Res. 60, e2023WR036521. https://doi.org/10.1029/2023WR036521.

Maza, M., Lara, J.L., Losada, I.J., 2021. Predicting the evolution of coastal protection service with mangrove forest age. Coast. Eng. 168, 103922. https://doi.org/10.1016/j.coastaleng.2021.103922.

Möller, I., Kudella, M., Rupprecht, F., Spencer, T., Paul, M., Van Wesenbeeck, B.K., Wolters, G., Jensen, K., Bouma, T.J., Miranda-Lange, M., Schimmels, S., 2014. Wave attenuation over coastal salt marshes under storm surge conditions. Nat. Geosci. 7, 727–731. https://doi.org/10.1038/ngeo2251.

Morris, R.L., Konlechner, T.M., Ghisalberti, M., Swearer, S.E., 2018. From grey to green: efficacy of eco-engineering solutions for nature-based coastal defence. Glob. Chang. Biol. 24, 1827–1842. https://doi.org/10.1111/gcb.14063.

Mortensen, E., Tiggeloven, T., Kiesel, J., Ward, P.J., 2024. For resilient rural shorelines: reviewing Nature-Based Solutions for flood risk reduction in small coastal communities. Nature-Based Solutions 6, 100189. https://doi.org/10.1016/j.nbsj.2024.100189.

Muñoz, D.F., Yin, D., Bakhtyar, R., Moftakhari, H., Xue, Z., Mandli, K., Ferreira, C., 2022. Inter-model comparison of Delft3D-FM and 2D HEC-RAS for Total water level prediction in coastal to inland transition zones. JAWRA J. Am. Water Resour. Assoc. 58, 34–49. https://doi.org/10.1111/1752-1688.12952.

Nederhoff, K., Saleh, R., Tehranirad, B., Herdman, L., Erikson, L., Barnard, P.L., Van Der Wegen, M., 2021. Drivers of extreme water levels in a large, urban, high-energy coastal estuary – a case study of the San Francisco Bay. Coast. Eng. 170, 103984. https://doi.org/10.1016/j.coastaleng.2021.103984.

Neumeier, U., 2007. Velocity and turbulence variations at the edge of saltmarshes. Cont. Shelf Res. 27, 1046–1059. https://doi.org/10.1016/j.csr.2005.07.009.

Reimann, L., Vafeidis, A.T., Honsel, L.E., 2023. Population development as a driver of coastal risk: current trends and future pathways. Camb. Prisms Coast. Futur. 1, e14. https://doi.org/10.1017/cft.2023.3.

Roy, S., Chakraborty, U., 2014. Salt tolerance mechanisms in salt tolerant grasses (STGs) and their prospects in cereal crop improvement. Bot. Stud. 55, 31. https://doi.org/10.1186/1999-3110-55-31.

Rupprecht, F., Möller, I., Paul, M., Kudella, M., Spencer, T., Van Wesenbeeck, B.K., Wolters, G., Jensen, K., Bouma, T.J., Miranda-Lange, M., Schimmels, S., 2017. Vegetation-wave interactions in salt marshes under storm surge conditions. Ecol. Eng. 100, 301–315. https://doi.org/10.1016/j.ecoleng.2016.12.030.

Saleh, F., Weinstein, M.P., 2016. The role of nature-based infrastructure (NBI) in coastal resiliency planning: a literature review. J. Environ. Manag. 183, 1088–1098. https://doi.org/10.1016/j.jenvman.2016.09.077.

Schoutens, K., Heuner, M., Minden, V., Schulte Ostermann, T., Silinski, A., Belliard, J., Temmerman, S., 2019. How effective are tidal marshes as nature-based shoreline protection throughout seasons? Limnol. Oceanogr. 64, 1750–1762. https://doi.org/10.1002/lno.11149.

Schoutens, K., Heuner, M., Fuchs, E., Minden, V., Schulte-Ostermann, T., Belliard, J.-P., Bouma, T.J., Temmerman, S., 2020. Nature-based shoreline protection by tidal marsh plants depends on trade-offs between avoidance and attenuation of hydrodynamic forces. Estuar. Coast. Shelf Sci. 236, 106645. https://doi.org/10.1016/j.ecss.2020.106645.

Schuerch, M., Mossman, H.L., Moore, H.E., Christie, E., Kiesel, J., 2022. Invited perspectives: managed realignment as a solution to mitigate coastal flood risks – optimizing success through knowledge co-production. Nat. Hazards Earth Syst. Sci. 22, 2879–2890. https://doi.org/10.5194/nhess-22-2879-2022.

Seenath, A., Romeo Mahadeo, S.M., Catterson, J., 2025. Public perceptions of nature-based coastal solutions in the UK. J. Environ. Manag. 373, 123413. https://doi.org/10.1016/j.jenvman.2024.123413.

SEPA, 2021. Flood Risk Management Plan. Forth Estuary Local Plan District.

Sheng, Y.P., Lapetina, A., Ma, G., 2012. The reduction of storm surge by vegetation canopies: three-dimensional simulations. Geophys. Res. Lett. 39, 2012GL053577. https://doi.org/10.1029/2012GL053577.

Sheng, Y.P., Rivera-Nieves, A.A., Zou, R., Paramygin, V.A., 2021. Role of wetlands in reducing structural loss is highly dependent on characteristics of storms and local wetland and structure conditions. Sci. Rep. 11, 5237. https://doi.org/10.1038/s41598-021-84701-z.

Silinski, A., Fransen, E., Bouma, T.J., Meire, P., Temmerman, S., 2016. Unravelling the controls of lateral expansion and elevation change of pioneer tidal marshes. Geomorphology 274, 106–115. https://doi.org/10.1016/j.geomorph.2016.09.006.

Smolders, S., Plancke, Y., Ides, S., Meire, P., Temmerman, S., 2015. Role of intertidal wetlands for tidal and storm tide attenuation along a confined estuary: a model study. Nat. Hazards Earth Syst. Sci. 15, 1659–1675. https://doi.org/10.5194/nhess-15-1659-2015.

Sonnenwald, F., Stovin, V., Guymer, I., 2019. Estimating drag coefficient for arrays of rigid cylinders representing emergent vegetation. J. Hydraul. Res. 57, 591–597. https://doi.org/10.1080/00221686.2018.1494050.

Sutton-Grier, A.E., Wowk, K., Bamford, H., 2015. Future of our coasts: the potential for natural and hybrid infrastructure to enhance the resilience of our coastal communities, economies and ecosystems. Environ. Sci. Pol. 51, 137–148. https://doi.org/10.1016/j.envsci.2015.04.006.

Tang, B., Gallien, T.W., 2023. Predicting compound coastal flooding in embayment-backed urban catchments: seawall and storm drain implications. J. Mar. Sci. Eng. 11, 1454. https://doi.org/10.3390/jmse11071454.

Taylor-Burns, R., Reguero, B.G., Barnard, P.L., Beck, M.W., 2025. Nature-based solutions extend the lifespan of a regional levee system under climate change. Sci. Rep. 15, 16218. https://doi.org/10.1038/s41598-025-99762-7.

Temmerman, S., Horstman, E.M., Krauss, K.W., Mullarney, J.C., Pelckmans, I., Schoutens, K., 2023. Marshes and mangroves as nature-based coastal storm buffers. Annu. Rev. Mar. Sci. 15, 95–118. https://doi.org/10.1146/annurev-marine-040422-092951.

Van Coppenolle, R., Schwarz, C., Temmerman, S., 2018. Contribution of mangroves and salt marshes to nature-based mitigation of coastal flood risks in major deltas of the world. Estuar. Coasts 41, 1699–1711. https://doi.org/10.1007/s12237-018-0394-7.

Vargas-Luna, A., Crosato, A., Calvani, G., Uijttewaal, W.S.J., 2016. Representing plants as rigid cylinders in experiments and models. Adv. Water Resour. 93, 205–222. https://doi.org/10.1016/j.advwatres.2015.10.004.

Villasante, S., Richter, K., Bailey, J., Blenckner, T., Farrell, E., Mongruel, R., Timmermann, K., Bouma, T., Melaku Canu, D., Chen, M., Lachs, L., Payo, A., Sousa Pinto, I., 2023. Building coastal resilience in Europe. In: Alexander, B., Muñiz Piniella, A., Kellett, P., Rodriguez Perez, A., Van Elslander, J., Bayo Ruiz, F., Heymans, J.J. (Eds.), Position Paper N°. 27 of the European Marine Board, Ostend, Belgium. https://doi.org/10.5281/zenodo.8224055 (126pp. ISSN: 0167–9309. ISBN: 9789464206197).

Wadey, M.P., Haigh, Ivan.D., Nicholls, R.J., Brown, J.M., Horsburgh, K., Carroll, B., Gallop, S.L., Mason, T., Bradshaw, E., 2015. A comparison of the 31 January–1 February 1953 and 5–6 December 2013 coastal flood events around the UK. Front. Mar. Sci. 2. https://doi.org/10.3389/fmars.2015.00084.

Williams, J.J., Esteves, L.S., 2017. Guidance on setup, calibration, and validation of hydrodynamic, wave, and sediment models for shelf seas and estuaries. Adv. Civ. Eng. 2017, 1–25. https://doi.org/10.1155/2017/5251902.

Yamanaka, Y., Matsuba, Y., Tajima, Y., Shibata, R., Hattori, N., Wu, L., Okami, N., 2019. Nearshore dynamics of storm surges and waves induced by the 2018 typhoons Jebi and Trami based on the analysis of video footage recorded on the coasts of Wakayama, Japan. J. Mar. Sci. Eng. 7, 413. https://doi.org/10.3390/jmse7110413.

Yin, J., Lin, N., Yu, D., 2016. Coupled modeling of storm surge and coastal inundation: a case study in N ew Y ork C ity during H urricane S andy. Water Resour. Res. 52, 8685–8699. https://doi.org/10.1002/2016WR019102.

Yin, K., Xu, S., Huang, W., Liu, S., Li, M., 2021. Numerical investigation of wave attenuation by coupled flexible vegetation dynamic model and XBeach wave model. Ocean Eng. 235, 109357. https://doi.org/10.1016/j.oceaneng.2021.109357.

Zhao, H., Chen, Q., 2016. Modeling attenuation of storm surge over deformable vegetation: parametric study. J. Eng. Mech. 142, 06016006. https://doi.org/10.1061/(ASCE)EM.1943-7889.0001109.